

Structural changes during the formation of gold single-atom chains: Stability criteria and electronic structure

F. Tavazza, L. E. Levine, and A. M. Chaka

National Institute of Standards and Technology, Gaithersburg, Maryland 20899, USA

(Received 30 September 2009; published 17 June 2010)

Under tensile deformation, Au nanowires (NWs) elongate to form single atom chains via a series of intermediate structural transformations. These intermediate structures are investigated using *static* density-functional theory, with particular attention paid to their behavior under load. The accessibility of these structures and their stability under load are found to be key factors governing the morphological evolution of the NW, while the ground-state energy of the *unstrained* structures does not correlate well with the observed behavior. Reverse loading conditions are also studied, where a NW is first deformed in tension and then deformed in compression. Again, accessibility and stability under load are the key criteria for predicting the evolution of the NW. Finally, electronic structure studies show abrupt opening and closing of small band gaps during tensile deformation, possibly explaining conductance oscillations observed experimentally. An analysis of the orbital interactions responsible for this unusual band-gap behavior is presented.

DOI: [10.1103/PhysRevB.81.235424](https://doi.org/10.1103/PhysRevB.81.235424)

PACS number(s): 61.46.Km, 64.70.Nd, 62.25.-g, 73.63.-b

I. INTRODUCTION

The formation and electrical properties of Au single atom chains (SAC) have attracted considerable attention from the scientific community, both for fundamental studies of the electrical and mechanical behavior of few-atom systems, and for their enormous potential as interconnects in future atomic-size electrical devices.^{1–12} In addition, the reproducible breaking strength of Au SACs make them promising candidates for intrinsic force calibration standards.¹³

All Au SACs are formed by a ductile thinning process during tensile deformation.^{14–19} Considerable modeling work^{20–53} has been devoted to the investigation of such wires, with particular attention to the relationship between wire thinning and conductance values. A few review works on the subject have been written as well.^{54,55} The structural changes that occur during the final stages of elongation to a SAC have also been extensively examined,^{11,47,56} but disagreement remains as to which atomic configuration is most stable at that stage.^{19,57–60} In addition to this still being an open question, little attention has been paid to the morphology of the intermediate stages in the nanowire (NW) evolution. Moreover, stability calculations for possible intermediate/final structures have often been conducted using relaxed (unstrained) atomic configurations. In particular, a recent static characterization of possible intermediate atomic structures for elongated Au NWs found a band gap for one particular configuration.⁴⁶ However, these simulations were conducted using very idealized conditions (infinite chain, unloaded conditions) and did not address the accessibility of these structures during a tensile deformation experiment, or the stability of the structure itself under tensile load conditions.

We recently used static density-functional theory (DFT) to explore the structural evolution of Au NWs during tensile deformation under a wide range of conditions, including high- and low-symmetry axes, different nanowire shapes, and different effective strain rates. A rich diversity of structural transitions was found, and four apparently stable intermediate atomic structures were identified.¹³ In this paper, we

use DFT to explore the stability (under load) and electronic properties of these intermediate atomic structures and of other possible structures reported in the literature. We find that the sequence of structural transitions that result in SAC formation depends upon three important factors: structural accessibility, i.e., the presence of an energetically reasonable deformation path from a previous configuration to the structure under examination, stability of such a structure under load, and low energy under the constraint of fixed wire length and number of atoms.

To further investigate the accessibility and stability of such structures, the reversibility of the elongation process has been analyzed. In all cases examined, if the deformation path is changed from tension to compression at some point in the simulation, bonds that had just broken are reformed. Moreover, upon compressing a SAC over a limited range, we observed the formation of ordered two-dimensional (2D) structures, although the sequence of structures formed did not always mirror those observed during tensile loading. Again, accessibility, stability under the applied load and low energy must be considered together to understand why a particular structure is formed. All of these findings agree with experimental structural observations,¹⁹ as well as with measures of conductance for Au NWs, where very similar plateaus for the quantum conductance are found before the single atom contact is broken, and after it has been broken and reformed again.⁶¹

Lastly, electronic properties of all accessible intermediate structures were computed, and the opening of a small gap (about 0.4 eV) was found when a small amount of the previously reported⁴⁶ ZZ3+5 structure developed during elongation. This is a much smaller gap than that found for the ideal, infinite ZZ3+5 structure (1.3 eV),⁴⁶ but it was obtained using much more realistic structural and elastic strain conditions.

The paper is organized as follows. The details of our simulations are discussed in Sec. II, and our results are presented in Sec. III, starting with the analysis of the relative stability and accessibility of the various structures under tensile conditions in Sec. III A. The local reversibility of the

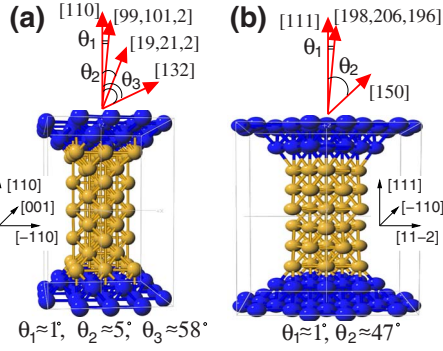


FIG. 1. (Color online) Initial structures for our cluster simulations. Darker circles (blue online) indicate grip atoms, while lighter ones (yellow online) are atoms allowed to move during the simulation. Most of the considered tensile axes are indicated above the cells (in red online). a) [110] NW, b) [111] NW.

elongation and the evolution of the SAC under compression are discussed next in Sec. III B, followed by the investigation of the electronic properties in Sec. III C. Lastly, our conclusions are summarized.

II. METHOD

The structural evolution and electronic properties of the intermediate atomic configurations were explored using static DFT simulations of infinite-length chains with one-dimensional periodic boundary conditions. As described in detail in Ref. 13, the computations were conducted using DMol³,^{62,63} where the physical wave function is expanded in an accurate numerical basis set.⁶⁴ We used a real-space cutoff of 0.4 nm and a double-zeta, atom-centered basis set (dnd). A generalized gradient approximation approach (Perdew-Burke-Ernzerhof⁶⁵) was used, along with a hardness conserving semilocal pseudopotential [dspp (Ref. 66)], where only electrons with $n=5$ and $n=6$ were handled explicitly. Lastly, geometry optimization was performed using a conjugate gradient approach based on a delocalized internal coordinate scheme.^{67,68}

In our previous paper,¹³ we investigated the elongation of Au NWs by statically applying tensile strain in very small increments to initial structures such as those shown in Fig. 1, i.e., NWs with wire axes along [110] or [111] crystallographic orientations, that are elongated along high- or low-symmetry tensile axes. The top and bottom two (or more) planes constituted the grips, which were incrementally moved along the tensile axis at each elongation step. After each tensile increment, the grip atoms were kept fixed while all of the other atoms were allowed to relax into new configurations. For all simulations, we utilized a finite cluster configuration to easily investigate different pulling mechanisms (both single and double sided stretching modes were used), and to eliminate self-interactions between the ends of the chain. In the following we will refer to these as the “cluster” simulations. Numerous cell shapes, sizes, and tensile axes were studied, in addition to those depicted in Fig. 1.

As a result of the cluster simulations described above, four apparently stable intermediate atomic configurations

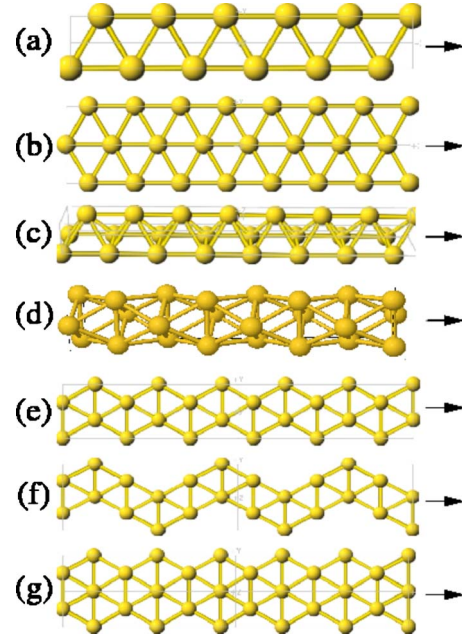


FIG. 2. (Color online) 1D infinite-length chains: (a) “Zig-Zag,” often seen in the literature (Refs. 58, 69, and 70) and found in our cluster simulations; (b) “Hexagonal,” found in our cluster simulations; (c) “Triangular110,” found in our [110]-wire cluster simulations; (d) “Triangular111,” found in our [111]-wire cluster simulations; (e) “ZZ3+5,” a modification of the rotated hexagonal phase, as proposed in Ref. 46, (f) “ZZ3+5-mod,” modification of ZZ3+5; and (g) “Hexagonal-mod,” rotated hexagonal phase. The arrow indicates the loading direction.

were frequently found during the elongation process.¹³ These structures will be referred to as “Zigzag,” “Hexagonal,” “Triangular110,” and “Triangular111,” and they are shown in Figs. 2(a)–2(d). A small amount of structure “ZZ3+5” was found as well [Fig. 2(e)]. To better understand the stability of such structures, and to compare their stability under tensile loading to that of other possible configurations that have been proposed in the literature,⁴⁶ we computed structural and electronic properties for several such configurations.

All of the structures we examined are shown in Fig. 2. Structure (a) is the commonly studied “Zig-Zag” structure,^{19,58,69,70} structure (b) is a hexagonal structure (“Hexagonal”) oriented as we found it in the course of our cluster simulations, structure (c), “Triangular110,” is the only nonplanar stable intermediate structure that we encountered in our [110]-oriented wire cluster simulations (note that this structure is a conventional triangular truss design used for construction), and structure (d) is a stable intermediate nonplanar structure that occurs frequently during the elongation of our [111]-oriented wire (“Triangular111”). Structure (e) was proposed in Ref. 46, where it was named “ZZ3+5,” and it is of great interest because it exhibits a semiconductorlike electronic structure. Structure (f) (ZZ3+5-mod) is a variation of structure (e) that we explored for completeness sake, and finally, structure (g) is a rotated hexagonal structure (“Hexagonal-mod”), that is related to “ZZ3+5.” Thus, the structures in Figs. 2(a)–2(d) were extensively found in our earlier cluster nanowire stretching simulations, and structures

in Figs. 2(a) and 2(e) were previously discussed in the literature.

To make energy comparisons as straightforward as possible, we considered the same size cell wherever structurally allowed. Therefore, we used 24 atom cells for the structures in Figs. 2(a)–2(f), and a 25 atom cell for the structure in Fig. 2(g). In all simulations, we considered an infinite chain configuration, i.e., we eliminated the grips and considered a cell with one-dimensional (1D) periodic boundary conditions. In DMol³ it is not possible to apply periodic boundary conditions along one direction only, so a configuration with 1D periodic boundary conditions is obtained considering a three-dimensional (3D) periodic cell with the correct length in the direction of real periodicity, and large amounts of vacuum along the remaining two directions. However, because in DMol³ the wave function is expanded in a numerical basis set, the addition of vacuum does not increase the computational cost of the calculations. Therefore, we considered very large (200 Å) cells in the lateral directions, so that no interaction between a cell and its image would affect our results. For all 24-atom cell calculations we used 5 Monkhorst-Pack k -points⁷¹ in the periodic direction when performing the elongation simulations, and 11 Monkhorst-Pack k -points when analyzing the total and partial density of states (DOS and pDOS, respectively) of the system.

The energy gaps discussed in Sec. III C were computed from band structure calculations, where 100 k -points were used along the Γ - X direction. Extensive tests were performed to guarantee convergence in k points for all our results. The highest occupied molecular orbitals (HOMOs) displayed in Fig. 14 were computed in Gamma.

At each tensile step, the cell size along the tensile axis direction was incremented by a fixed amount, and all of the atoms in the cell were allowed to relax into a new configuration. This methodology has been extensively used in recent years when studying nanowire deformation.⁷² Usually, the system was considered converged when the change in total energy per atom was less than 1×10^{-6} eV and the atomic forces were less than 0.001 eV/Å. Different effective strain rates were simulated by slightly changing the convergence criteria on the gradient of the atomic positions, similar to the procedure in Picaud *et al.*⁷³ Thus, the most stringent convergence criteria produce highly converged structures that correspond to real systems that were strained slowly enough to allow complete relaxation. Slightly less stringent convergence criteria approximate higher strain rates where the system has less time to relax. This procedure is used to explore the possible effects of strain rate on this system, and no quantitative correspondence to real physical strain rates is implied. Because calculations were much faster for these 1D cases than for the cluster calculations, many more effective strain rate and tensile axis variations were investigated. As in the cluster calculations, slightly off-axis (i.e., low symmetry) tensile axes were predominantly used to guarantee that no artificially symmetric deformation path was imposed during deformation.

III. RESULTS

A. Stability and accessibility of stable intermediate structures

As reported previously,¹³ four apparently stable intermediate atomic configurations (“Zigzag,” “Hexagonal,” “Tri-

TABLE I. Intrinsic wire length for different 24-atom structures: (A) all structures have a nearest-neighbor (nn) distance equal to 2.88 Å, (B) wire length corresponding to the zero stress, minimum energy configuration.

Structure	Wire length (Å)	
	(A)	(B)
Zig-Zag	34.5608	32.5428
ZZ3+5	29.9305	27.0848
Hexagonal	23.0405	22.0414
Triangular110	23.0405	21.7728
Triangular111	18.4804	17.1488

gular110,” and “Triangular111,” Fig. 2) were found in a DFT-based structural study of Au nanowire deformation. The formation pathways for these structures involved large rearrangements of local atomic structure. We refer to Ref. 13 for examples of all those intermediate configurations as found during our cluster simulations, and of some of their formation pathways.

In the following, we investigate the energetic and structural properties of these intermediate structures, as well as those of other 2D configurations as described in Sec. II. Total energy minimization under elastic conditions will be discussed first, followed by more physically motivated energy comparisons between structures that are elongated under conditions that allow for plastic deformation.

As a first step in the characterization of these structures, we computed their total energy as a function of *isotropic* volume change. This approach was used by Fioravante *et al.*⁴⁶ to evaluate the relative stability of different atomic structures in Au nanowires. It is doubtful that such an analysis would provide reliable predictions since the imposed tensile deformation of a nanowire is highly directional and very different from an isotropic volume change. However, it allows for a very straightforward comparison between the various structures.

For the isotropic volume change calculation, all of the initial configurations were prepared such that the nearest-neighbor (nn) distance between atoms coincided with the nearest-neighbor distance in bulk Au (2.88 Å). As a consequence, the overall length of the wire was different from structure to structure [see Table I, column (A)]. These results are presented in Fig. 3. As shown in Fig. 3, the isotropic expansion approach predicts that the two-dimensional hexagonal structure (“Hexagonal”) is the most stable structure, followed by “Hexagonal-mod” (still two dimensional) for interatomic distances shorter than their bulk value, and by “Triangular111” (a three-dimensional configuration) for interatomic distances larger than their bulk value. The least stable structure is the commonly found “Zig-Zag.” This stability ranking does not correspond well with the structures observed in our simulations.¹³ Thus, the “Hexagonal-mod” structure was never seen in our cluster simulations or reported in the literature, while “Zig-Zag” is a well-known intermediate structure encountered while elongating Au

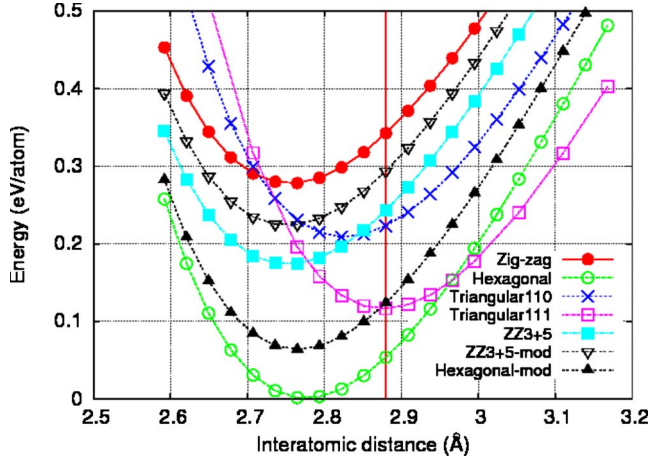


FIG. 3. (Color online) Energy versus nearest-neighbor distance obtained by imposing isotropic volume changes to several feasible intermediate structures. The vertical line in the figure indicates the bulk nearest neighbor distance.

nanowires. It is therefore clear that this isotropic volume change test does not capture the necessary physics and a more physically motivated approach is required.

As a second step toward understanding what determines the relative stability of these structures, we investigated the effect of purely elastic tensile deformation: considering just the unit cell of each structure, we strained it along the axial direction in such a way that all degrees of freedom were relaxed inside the unit cell and only the length of the cell remained as a boundary condition. Results of these calculations are shown in Fig. 4. The “Hexagonal” structure remains the most stable, followed by the “Triangular111,” and, again, the least stable is the “Zig-Zag” structure. However, compared to the isotropic results, small changes are found in the cross over points between the “Triangular111” and “Hexagonal-mod” structures, and also between the “Triangular110” and “ZZ3+5” ones. The average nearest-neighbors

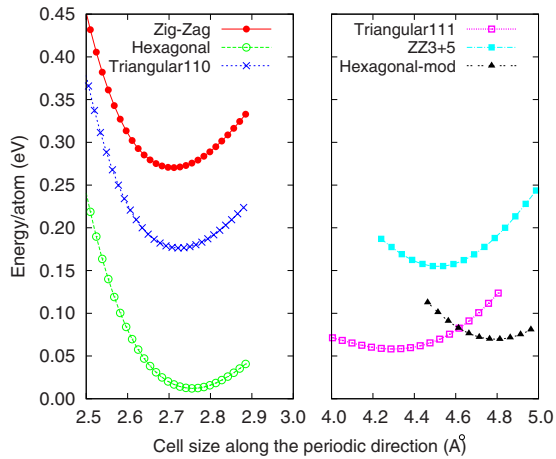


FIG. 4. (Color online) Energy versus cell size in the axial direction. The calculations were performed just for the unit cell of each structure, so that only elastic deformation was possible. At each step, all of the degrees of freedom were relaxed inside the unit cell while the length of the cell remained fixed as a boundary condition.

TABLE II. Average nearest-neighbor distance and wire length for different structures at zero stress. All calculations have been performed using the unit cell of each structure, i.e., only elastic deformation has been allowed. The structures are listed in order of stability.

Structure	Elastic deformation only (Å)	
	Average nn distance	Cell length
Hexagonal	2.775 ± 0.002	2.7552
Triangular111	2.887 ± 0.012	4.2872
Hexagonal-mod	2.767 ± 0.004	4.7885
ZZ3+5	2.762 ± 0.011	4.5141
Triangular110	2.839 ± 0.008	2.7216
Zig-Zag	2.761 ± 0.005	2.7119

distance for each structure in its minimal energy configuration (zero applied stress) is reported in Table II. For 2D structures, such interatomic distances are always smaller than their bulk value, and not much of a variation is observed among different structures. However, for 3D structures (“Triangular111” and “Triangular110”) the average nearest-neighbor distance approaches the bulk value, and a larger variation is observed among the two structures. For each structure, the wire length corresponding to the minimal energy is given in Table II for the unit cells, and in Table I for the 24-atom cells. Such 24-atom cells have also been used in simulations where both elastic and plastic deformation are allowed (see below). The need for such simulations is highlighted by the fact that, again, the stability ranking obtained considering only elastic effects does not agree with our previous findings.¹³

Three very important factors must be taken into consideration when trying to understand the intermediate stages of elongation. First, intermediate structures must be accessible. This means that there must be an energetically reasonable deformation path from a given initial structure to the structure under examination. Second, the structure must be stable under the imposed strain. This can only be tested by allowing structural rearrangements during deformation, and is therefore not included in elastic calculations. Third, because of the stretching, the length of the wire is constrained. There is no experimental evidence of a significant diffusion of atoms from the bulk to the elongating wire, so we may safely assume a constant number of atoms in the wire itself. Therefore, given a fixed number of atoms, it is not which structure is energetically most favorable at the ideal nearest-neighbor distance that counts, but which one is most favorable for the required wire length.

To include all of these factors in our investigation, we used incremental static DFT to elongate the different structures, similar to what was done for the cluster calculations. Only “Hexagonal,” “Triangular110,” “ZZ3+5,” “Zig-zag,” and “Triangular111” were investigated, since “Hexagonal-mod” and “ZZ3+5-mod” were never found in our cluster simulations or reported in the literature. For each structure, we performed two sets of simulations, one where the initial

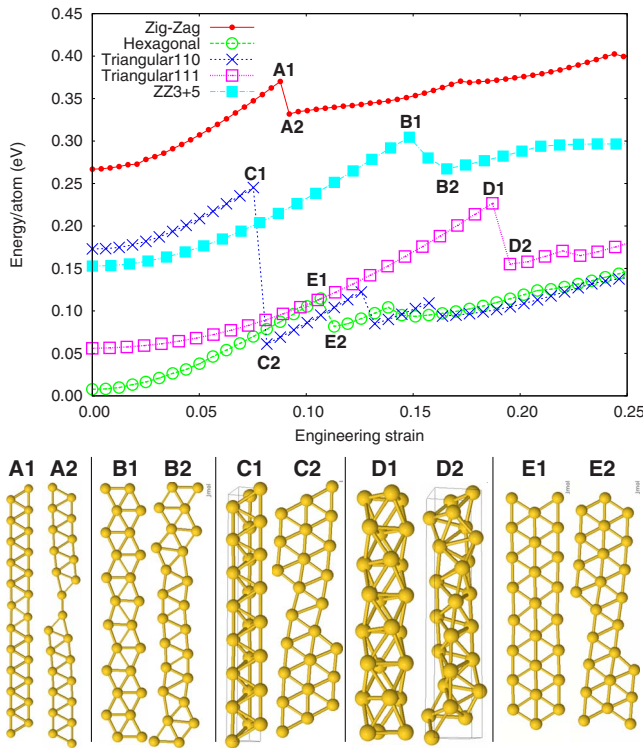


FIG. 5. (Color online) (Top) Plots of energy/atom versus engineering strain for the structures of interest. (Bottom) The configurations before and after the first structural rearrangement are shown for each initial structure.

structures had nearest-neighbor separations set to the bulk value, and a second set starting from the zero stress configurations determined using the elastic—only simulations (Fig. 4). Comparing these sets of simulations allowed us to evaluate, for each structure, how sensitive the evolution of the wire is to small elastic changes in the starting interatomic distances. For all of our structures, simulations conducted with exactly the same parameters but different initial interatomic distances showed no observable differences after the first few elongation steps.

In contrast to the cluster calculations, these structures were simulated as infinite chains, with periodic boundary conditions applied along the tensile direction. Thus, no grips were included, i.e., no atoms were constrained during the simulation. Several tensile axes, either along z or forming small angles ($\approx 1^\circ$ to 2°) with the z direction, were investigated. No significant difference in the evolution of the wire or breaking force was found as a function of the tensile axis. Several effective strain rates and step sizes were also investigated. General behaviors were found to be independent of these variables. However, lower strain rates and smaller elongation steps sometimes resulted in a larger number of atoms being involved in the structural phase transformations that occur during the elongation.

The plot in Fig. 5 shows the energy/atom during the early stages of elongation plotted versus the engineering strain ϵ [$\epsilon = (L - L_0)/L_0$, with L_0 and L being the initial and final NW lengths]. For each structure, the initial length corresponds to the 24-atom wire (Table I) in the minimum energy (zero

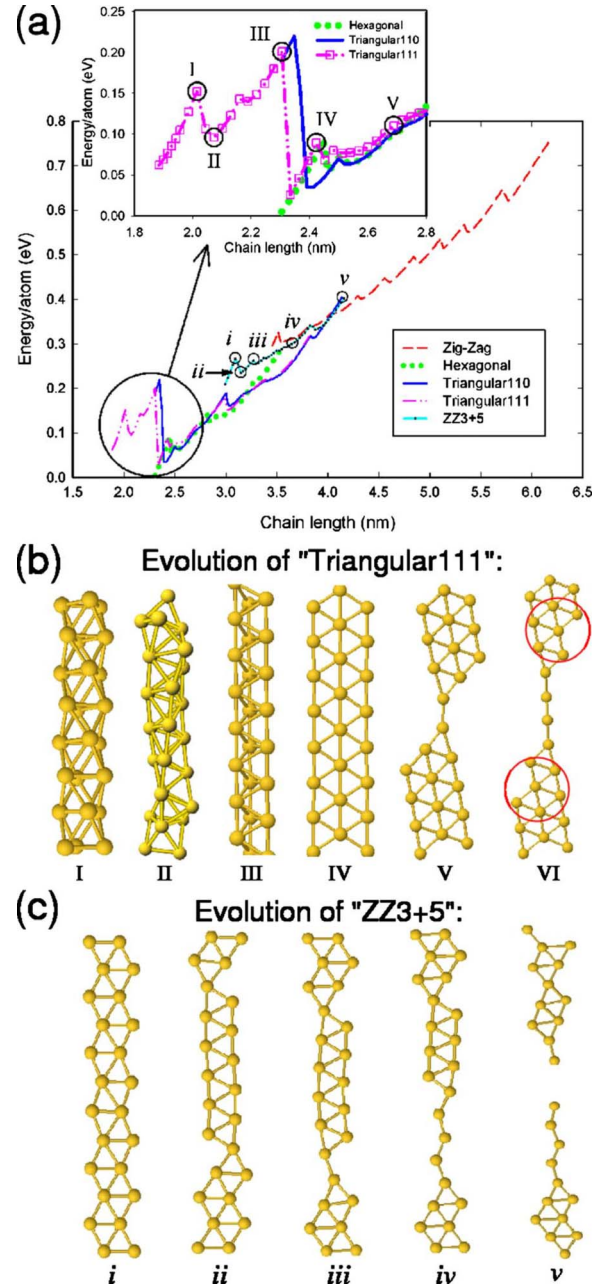
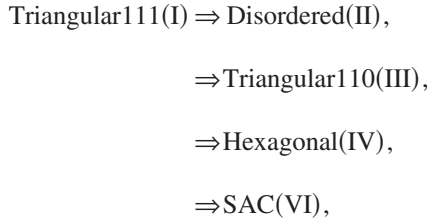


FIG. 6. (Color online) (a) Plots of energy/atom versus NW length. The runs are labeled with the name of the initial structure. During elongation, the initial configuration undergoes structural phase transformations corresponding to large, abrupt jumps in the energy curve. Examples of such transformations are shown in panels (b) and (c). (b) Evolution of the “Triangular111” structure to “Triangular110” (III), then to “Hexagonal” (IV), and finally a SAC (VI). In configuration (VI) a small amount of “ZZ3+5” (circled) can be seen. (c) The “ZZ3+5” structure quickly morphs into a “Zig-Zag” configuration (ii), then unzips and forms a SAC (iv).

applied stress) condition. As pointed out in the literature (Ref. 51 for instance), discontinuities in this energy curve correspond to structural changes; the corresponding atomic configurations are also shown in Fig. 5. In agreement with the elastic stability evaluation (Fig. 4), the “Triangular111” and “ZZ3+5” structures deform elastically up to a much

larger engineering strain than the less stable “Triangular110” and “Zig-Zag” structures. However, the “Hexagonal” structure, which is the most stable under solely elastic deformation, encounters its first structural transformation at a smaller engineering strain than the “Triangular111” or “ZZ3+5” structures. Overall, reasonable agreement is found for the other structures as well, between isotropic stability and duration of the elastic deformation.

The energetic behavior for the complete elongation process is presented in Fig. 6 for all structures of interest. Very interesting, and sometimes surprising, phase transformations occur. For example [see Fig. 6(b)], the “Triangular111” structure follows the deformation path



even though “Triangular110” is a higher energy configuration than “Triangular111.” Similarly, “ZZ3+5” quickly morphs into “Zig-Zag,” which is significantly less stable than “ZZ3+5” [see Fig. 6(c)]. All of these transitions can be understood in terms of accessibility and constrained dimensions, while remembering that uniaxial elastic deformation is not isotropic; thus, the Fig. 3 results are at best a guideline. As shown in Table I, “Triangular111” is the structure with the shortest intrinsic length. Therefore, it is reasonable to assume that it would evolve into some other structure that is less compact. “Triangular110” is structurally much closer to “Triangular111” than, for example “Hexagonal,” and it is, therefore, a good intermediate step. The most surprising aspect of this transformation is the recovery of a highly ordered structure (“Triangular110”) from an intermediate, disordered configuration. A measure of this disorder is given by the bond angle distribution shown in Fig. 7, where the three structures (“Triangular111,” disordered, and “Triangular110”) are compared.

From “Triangular110” the structural path to “Hexagonal” is relatively easy through a simple unzipping process and that is exactly what is seen in our simulations. Similarly, an easy deformation path connects “ZZ3+5” to “Zig-Zag” [see Fig. 6(b)], and this transformation occurs for elongations large enough to make it energetically convenient (the “Zig-Zag” structure has a larger intrinsic length than “ZZ3+5”). For faster effective strain rates, the same structural deformation path (i.e., sequence of structures) was usually seen, but only a limited number of atoms would participate in the structural rearrangement. One example of such behavior is shown in Fig. 8(a), where the initial structure (“Triangular111”) transforms only locally into “Triangular110” first, and “Hexagonal” later. This evolution path should be compared to that displayed in Fig. 6(b), where the elongation proceeded at a lower effective strain rate and all of the atoms participated in the transformation. Finally, it is important to note that both Figs. 6(b) and 8 show the formation of a limited amount of the “ZZ3+5” structure (slightly larger in Fig. 8). This proves

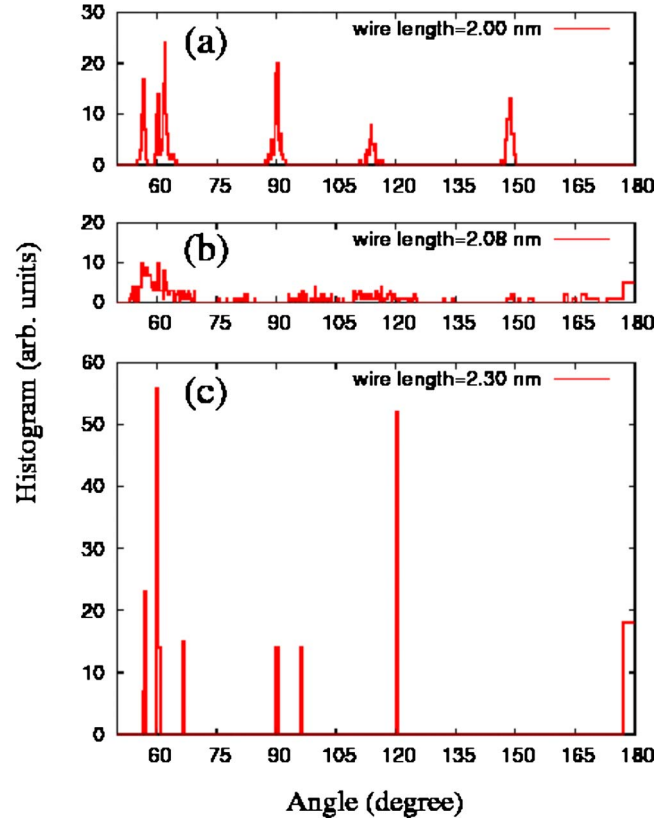


FIG. 7. (Color online) Angle distribution for three configurations along the “Triangular111” elongation path: (a) wire length = 2 nm gives the elastically deformed “Triangular111” structure shown in Fig. 6(b) I, (b) wire length = 2.08 nm produces the partially disordered structure shown in Fig. 6(b) II, and (c) wire length = 2.3 nm gives the “Triangular110” structure shown in Fig. 6(b) III.

the accessibility of the “ZZ3+5” structure, which may be of technological importance due to its semiconductor properties.

At this point, it is important to compare the structural deformation paths found for infinite chains with 1D periodic boundary conditions to those seen in the cluster calculations. A consistency between the two sets of results would further guarantee that limitations in the method (such as the chosen contact shape or size in the cluster simulations, or cell size in the chain simulations) have not significantly affected our results. In general, all of the structural transitions seen using the infinite chains have also been seen in the cluster calculations, but usually involving a smaller number of atoms. As an example, Fig. 8(b) shows a cluster calculation of the evolution of a [110]-NW from a “Triangular110” local structure into an “Hexagonal” one, and finally the formation of a very small amount of “ZZ3+5.”

Finally, we computed and compared the average nearest-neighbor distances for representative structures in all of the considered cases: cluster simulations for [110]- and [111]-cells and infinite chains; results are shown in Fig. 9 for a few of these cases. The initial positions for all of the cluster simulations were those of a perfect fcc lattice, either (110) or (111)-oriented [Fig. 9(d)]. The labels used in Figs. 9(b) and

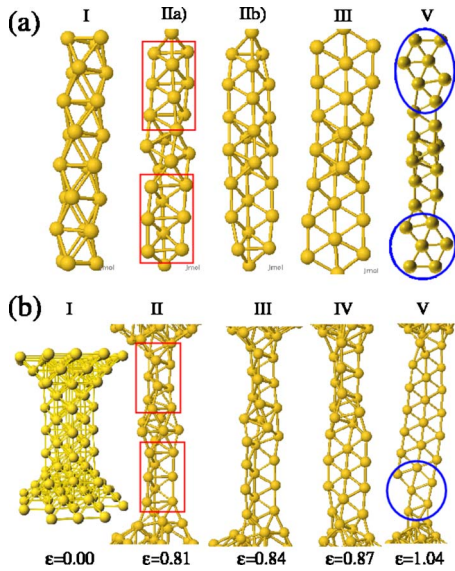


FIG. 8. (Color online) (a) Evolution of “Triangular111” obtained using an effective strain rate faster than in Fig. 6(b): the structural transitions are the same in both cases but here they only occur locally (i.e., they did not span the whole chain). Also, a larger amount of “ZZ3+5” structure is formed here (stage V, circled) than in the slower structural transition shown in Fig. 6(b). (b) Evolution of a [110]-cell into “Triangular110” (II) and “Hexagonal” (v), obtained using cluster calculations. ϵ is the engineering strain. In (b) V, a small amount of “ZZ3+5” is also visible (circled).

9(c) to indicate the different simulations refer to the intermediate structure that developed, in the central part of the chain, during the elongation process. Therefore, for the cluster simulations, only atoms initially in the central part of the wire are considered in this analysis [Fig. 9(d)]. Conversely, all of the atoms are considered when analyzing infinite chain results. Overall, good agreement between the two sets of calculations is found. In all cases the largest average nearest-neighbor distance found is about 2.94 Å, which corresponds to a 2.1% increase from its bulk value. However, structures with nearest-neighbor distances larger or equal to the bulk value are not energetically favorable, and the atoms quickly rearrange in such a way to shorten their nearest-neighbor distance to a value lower than its bulk value of 2.88 Å.^{74,75} Considering the diminished dimensionality of the wire, and, especially, the reduced number of nearest neighbor’s in the elongated portion of the wire, this finding is in good agreement with the nearest-neighbor distance of about 2.50 Å found in the limiting case of a Au dimer.^{76–78} Also, the average nearest-neighbor distance always diminishes going from 3D structures to 2D structures. Examples of 3D configurations include all of the data points up to an engineering strain of 0.9 for the [110]-cell [Fig. 9(b)], or “Triangular111” up to an engineering strain of about 0.2 in the case of the infinite chains [Fig. 9(a)]. The average nearest-neighbor distance for 2D structures is found to be about 2.8 Å from infinite chain calculations, about 2.84 Å from [110]-cell cluster calculations and 2.86 Å from [111]-cell cluster calculations. Also, this does not depend significantly on the structure itself. The value found using infinite chain simulations is slightly lower than those found using cluster calcu-

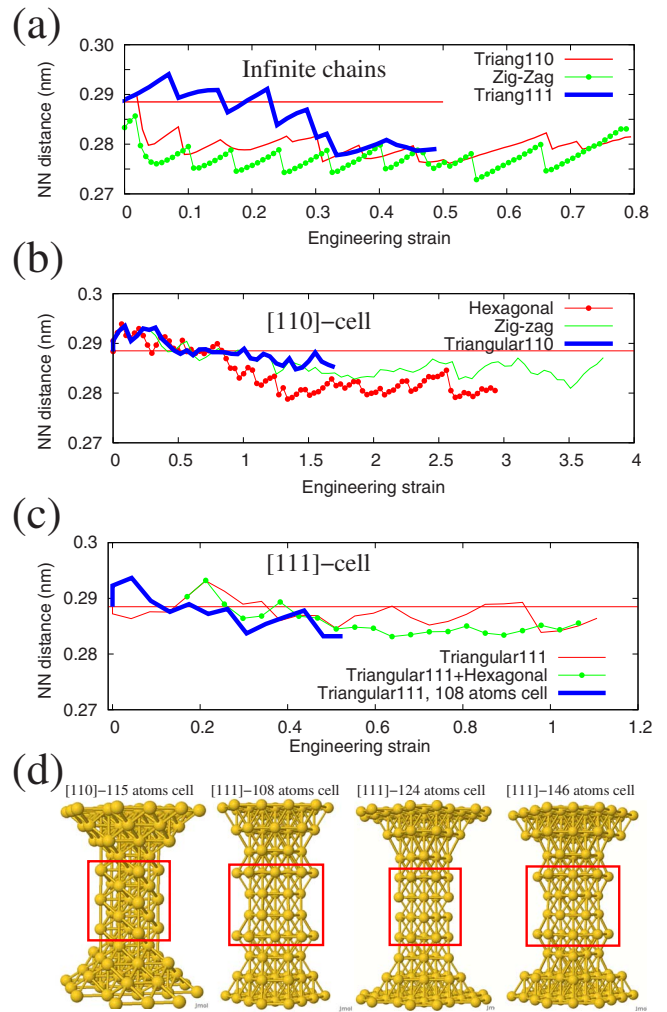


FIG. 9. (Color online) Average nearest-neighbor distances for: (a) infinite chain simulations, (b) cluster simulations for [110]-axis wires, and (c) cluster simulations for [111]-axis wires. (d) Simulation cells for the cluster calculations: the only nearest-neighbor distances considered in this analysis are those between atoms located in the central part of the wires [framed area (red online)]. The solid horizontal line in (a), (b), and (c) indicates the nearest-neighbor distance in bulk Au.

lations and shows smaller variability because all of the atoms participated in the structural transformation and belonged to the same 2D structure. Conversely, in the cluster simulation case, the constrained grips reduce the freedom of movement of the atoms in the central part of the wire, and in most cases some of the atoms included in the calculation have not contributed to the structural transformation.

B. Reversibility of the tensile deformation

To further characterize the morphological changes exhibited by the NWs during deformation, we investigated the reversibility of the structural transformations by reversing the load from tension to compression. This approach also provides further insight into the accessibility and stability of the different intermediate structures.

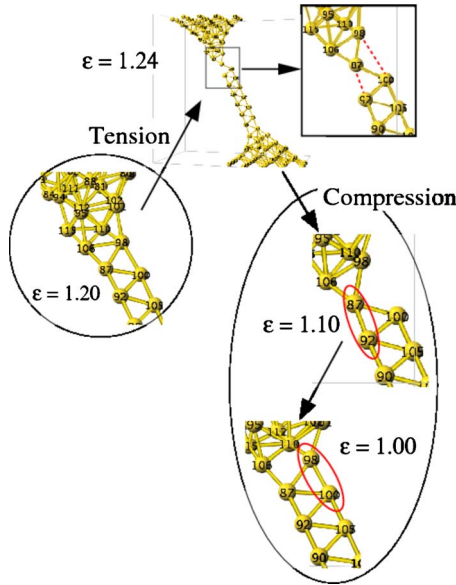


FIG. 10. (Color online) Example of reversibility observed during cluster simulations. Two bonds are broken during the tensile experiment (left), going from $\epsilon=1.20$ to $\epsilon=1.24$. The two broken bonds are represented by dashed lines. On the right the compression results are shown. One of the two broken bonds has reformed at $\epsilon=1.20$, while the other reformed later at $\epsilon=1.00$.

We studied reversibility using both cluster and infinite chain simulations. In particular, we investigated the reversibility of the structural transformation connecting 2D arrangements (“Hexagonal,” “ZZ3+5,” or “Zig-Zag”) to SACs. In these studies, we utilized configurations obtained during tensile deformation as initial configurations. Starting from such atomic positions, the wire was compressed at the same rate and along the same axis that had been used in the corresponding tensile experiment. For the cluster simulation results, the engineering strains are computed with respect to the length of the undeformed 3D structure displayed in Fig. 1, while the engineering strains for infinite chain simulations are computed with respect to the unstrained 24-atom wire length given in Table II.

In all cases examined, when the deformation path is changed from tension to compression, bonds that had just broken are reformed. An example of such a behavior is shown in Fig. 10, for a cluster simulation. Here the configuration obtained after 29 tensile increments ($\epsilon=1.24$) was used as the starting point for the compressive simulation. Both bonds that had broken during the last tensile step (dashed lines in the insert) are reformed in the compressive simulation, although some hysteresis is present, i.e., the bonds have reformed for engineering strains slightly different from those for which the bonds had broken under tensile conditions ($\epsilon=1.00$ instead of $\epsilon=1.20$).

More interesting results are found when long SACs are compressed. As depicted in Fig. 11, we find that a long SAC always folds up on itself during compression to form an ordered 2D structure. However, the nature of this structure is determined by the atomic arrangement immediately adjacent to the SAC, and thus the configuration present immediately prior to SAC formation. This can be seen by comparing Figs.

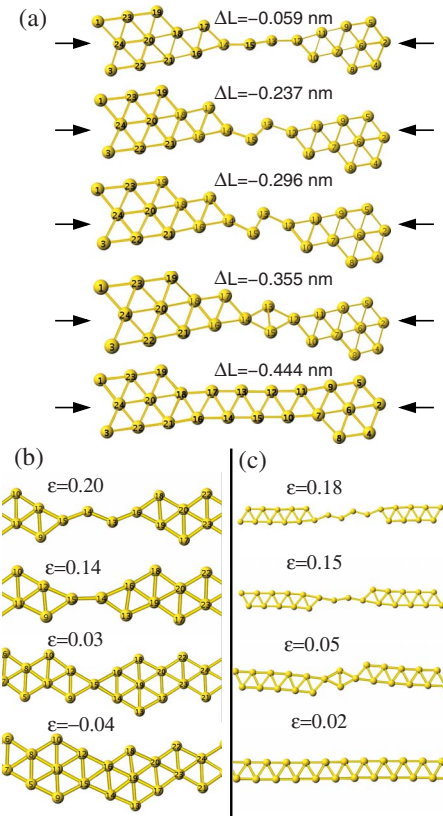


FIG. 11. (Color online) Examples of reversibility observed for infinite-chain simulations under compression conditions. The SAC folds into a 2D configuration that depends upon the atomic arrangement present immediately prior to SAC formation [a “Zig-Zag” in (a) and (c), and a ZZ3+5 in (b)]. The engineering strains for (b) and (c) are computed with respect to the 24-atom unstrained wires. For (a), the “Zig-Zag” structure formed through a structural transition so no such reference wire length is available. Here, the variation in wire length ($\Delta L=L-L_0$) is indicated, where L is the length of the compressed wire and L_0 is the wire length just before compression starts.

11(a) and 11(b): in both cases the SAC is 4 atoms long, but in (a), the “Zig-Zag” structure present prior to SAC formation is reformed, while in (b), a structure related to the original “ZZ3+5” is produced. This is completely analogous to what was found for the tensile case: it is the combination of accessibility, stability under the applied load and low energy that determines which structure gets formed.

It must be pointed out that the sequence of encountered structures is not necessarily reversible when going from a tensile experiment to a compressive one. This is primarily because the energy of a given structure strongly depends upon the imposed strain which is very different between uniaxial tension and compression. As an example, the SAC in Fig. 11(b) formed from the “ZZ3+5” structure during tension. Upon reversing the applied load, a limited amount of “Hexagonal-Mod” [see Fig. 2(g)] developed. “Hexagonal-Mod” was never observed in any of our tensile cluster simulations, but its low energy for short nearest-neighbor distances (see Fig. 4 and Table II) makes it a promising structure for compressive deformation. This, together with

the easy deformation path from a broken “ZZ3+5,” explains its appearance in this simulation. Figure 11(c) demonstrates that the folding of a SAC to an ordered 2D structure occurs for longer chains as well, and that the constituent atoms of the SAC are reabsorbed back into the contacts, as suggested in Ref. 19.

C. Electronic properties

Since electron orbital interactions depend strongly upon the local atomic structure, we examined how the basic electronic properties of our strained nanowires changed under the strain imposed during deformation. In particular, we focused on how the application of a tensile strain would affect the presence of a band gap in the “ZZ3+5” structure, which displays a significant band gap ($E_g=1.3$ eV) under unstrained conditions.⁴⁶ Similarly, we investigated the possibility that some of the other structures shown in Figs. 2(a)–2(e) could open a band gap during tensile evolution.

Our results can be summarized as follows. During tensile experiments, simulations starting from “Zig-Zag” and “Hexagonal” structures never displayed a band gap, while a gap often appeared for intermediate configurations during simulations with “Triangular110” and “Triangular111” starting structures. As for the “ZZ3+5” structure, the initial band gap almost completely disappears during the early stages of elongation, and then reopens under particular structural circumstances, similar to the behavior seen for the “Triangular110” and “Triangular111” structures. In all cases, the observed band gaps are small (about 0.4 eV). The details of how a given structure opens a gap will be discussed later in this section, but in general, the presence of some amount of the “ZZ3+5” structure seems to be a prerequisite. No band gap was found for structures without some amount of “ZZ3+5,” but the presence of some “ZZ3+5” would not, alone, guarantee the opening of a gap.

The top part of Fig. 12 shows the size of the band gap plotted as a function of the engineering strain for “Triangular110,” “Triangular111,” and “ZZ3+5” starting structures. Since different effective strain rates affect the specific atomic structures that evolve, the plots in Fig. 12 are not unique and only one example for each structure is shown; the examples were selected to show the wide range of behavior displayed by the wires. Very small band gaps (smaller than 0.2 eV for instance) may become irrelevant under finite temperature conditions. However, these gaps demonstrate that the electronic structure depends strongly on the details of the geometry, and strong scattering may occur when vibrations come into play. Structures corresponding to interesting features in the band gap plot are displayed in the lower part of the figure.

Starting with the evolution of the “ZZ3+5” structure, it is worth pointing out that the initial gap is about 0.9 eV instead of 1.3 eV. This is because, as discussed in Sec. II, the initial structures for our tensile simulations had nearest-neighbor distances set to the gold bulk value of 2.88 Å, instead of to the “ZZ3+5” equilibrium value of 2.76 Å (Sec. III A). Thus, the starting engineering strain is not zero. For a nearest-neighbor distance of 2.76 Å we found an energy gap

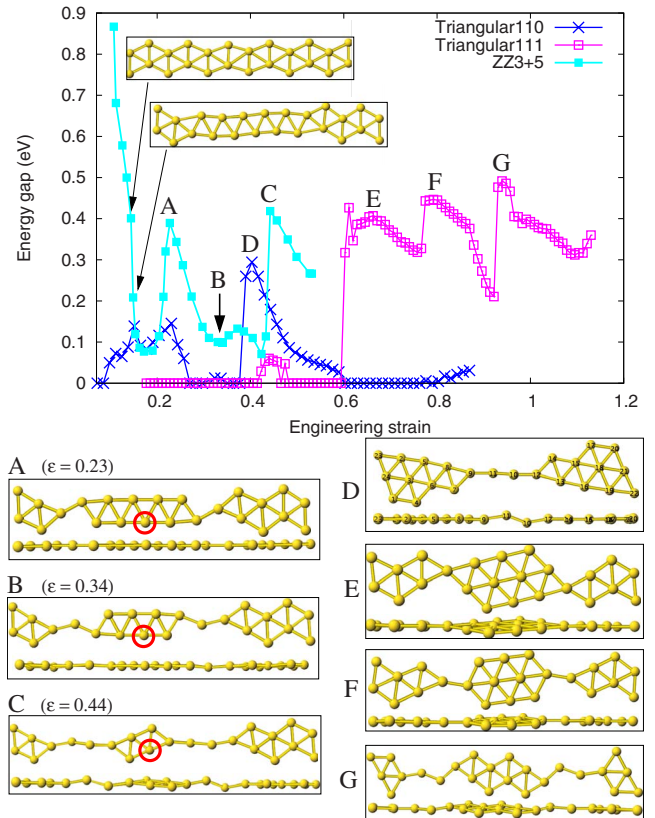


FIG. 12. (Color online) Examples of gap opening during the elongation process.

in very good agreement with Ref. 46. As the wire continues to stretch elastically up to an engineering strain of $\epsilon=0.14$, the gap reduces smoothly to 0.4 eV. At this strain, the first structural rearrangement occurs (see insets in the figure) and the gap abruptly reduces to 0.2 eV. As the wire continues to stretch, the gap remains very small for engineering strains between 0.14 and 0.21, then rapidly increases to a maximum of 0.4 eV when structure A in the figure forms. As before, this gap diminishes with increasing strain, becoming less than 0.2 eV for a large range of engineering strain before it reopens when structure C appears. The opening of a significant gap (between 0.3 and 0.5 eV) during elongation is also observed in most simulations for both the “Triangular110” and “Triangular111” starting structures. It is important to mention that in all cases when structural and electronic factors result in the opening of a gap, this gap noticeably reduces in size as the structure elongates elastically.

As mentioned above, changing the effective strain rate produces different atomic configurations that exhibit different electronic behaviors. Thus, while a band gap corresponding to structure A is found in all of our “ZZ3+5” simulations, the second reopening of the gap is observed in only some cases. Also, the “Triangular111” simulations usually displayed a band-gap opening behavior very similar to the one shown in Fig. 12 for the “Triangular110” structure, i.e., a single, limited gap opening, preceded and followed by conductive behavior.

The intermittent band-gap behavior observed during the nanowire simulations may help explain the abrupt up-and-

down conductance changes between zero and $1 G_0$ or $1.5 G_0$ that has been experimentally observed during tensile experiments (see Ref. 19 for instance). Here, $G_0=2e^2/h$ is the unit of quantum conductance, where e is the electron charge and h is Planck's constant. Definitive tests of this connection require quantum-mechanics-based simulations of electron transport within these deformed nanowires and direct comparison with experimental conductance measurements obtained under very similar conditions.⁶¹

It is also important to note that a recent theoretical study by Ke *et al.*⁴⁵ showed that simple rotational deformations of an infinite length, zigzagged SAC with constant lattice parameter lead to pronounced changes in the band structure and the opening and closing of a large band gap. Our findings confirm this dependence of the gap on the rotational arrangement of SAC atoms: using structure C in Fig. 12 as a test case, we found that rotating the two canted central atoms (see the lower in-plane picture in C) of the two SACs reduced the energy gap by half. However, the presence of a limited amount of “ZZ3+5” structure and the rotational arrangement of the atoms in the SAC still do not fully explain the opening of a band gap, as exemplified by the structural variety of small band gap configurations displayed in Fig. 12.

To deepen our understanding of the opening and closing of the band gap during the elongation process we focused our analysis on one particular simulation [the “ZZ3+5” simulation shown in Fig. 12], comparing two small-band-gap structures (A and C) to a conducting one (B), corresponding to an engineering strain intermediate between structures A and C. Note the pronounced structural similarity between all three configurations.

To determine why structure B is a conductor while A and C are not, we examined the density of states and atomic orbital contributions for structures A, B, and C, i.e., for engineering strains of 0.23, 0.34, and 0.44, respectively. As can be seen from Fig. 13(a), where the vertical lines indicate the position of the Fermi level for the s , p , and d orbitals, structure B has a significant density of states at the Fermi level in stark contrast to structures A and C. Projection of these states onto individual atoms indicates that the central zigzag region is responsible for the conduction band in structure B ($\epsilon=0.34$). This can be seen clearly in Fig. 13(b), which shows the projection of orbital components of states near the Fermi level onto atom 13, an atom that is central to the planar zigzag region in all three structures (atom 13 is circled in structures A, B, and C in Fig. 12). In structure A ($\epsilon=0.23$), the occupied states for the ten atoms in the zigzag region lie well below the Fermi level, thus introducing a significant band gap. The reason for this band gap can be clearly seen from the spatial projection of the orbital contribution for the highest occupied state of NW structure A shown in Fig. 14, which shows a highly localized, and thus insulating, character.

As the chain elongates to $\epsilon=0.34$ and the number of atoms in the zigzag region is reduced from ten to eight atoms, the energy of the occupied states increases to where the band straddles the Fermi level, thus closing the band gap [see Fig. 13(b)]. As the chain is further extended to $\epsilon=0.44$, the zigzag region is reduced to only six atoms and the energy of these

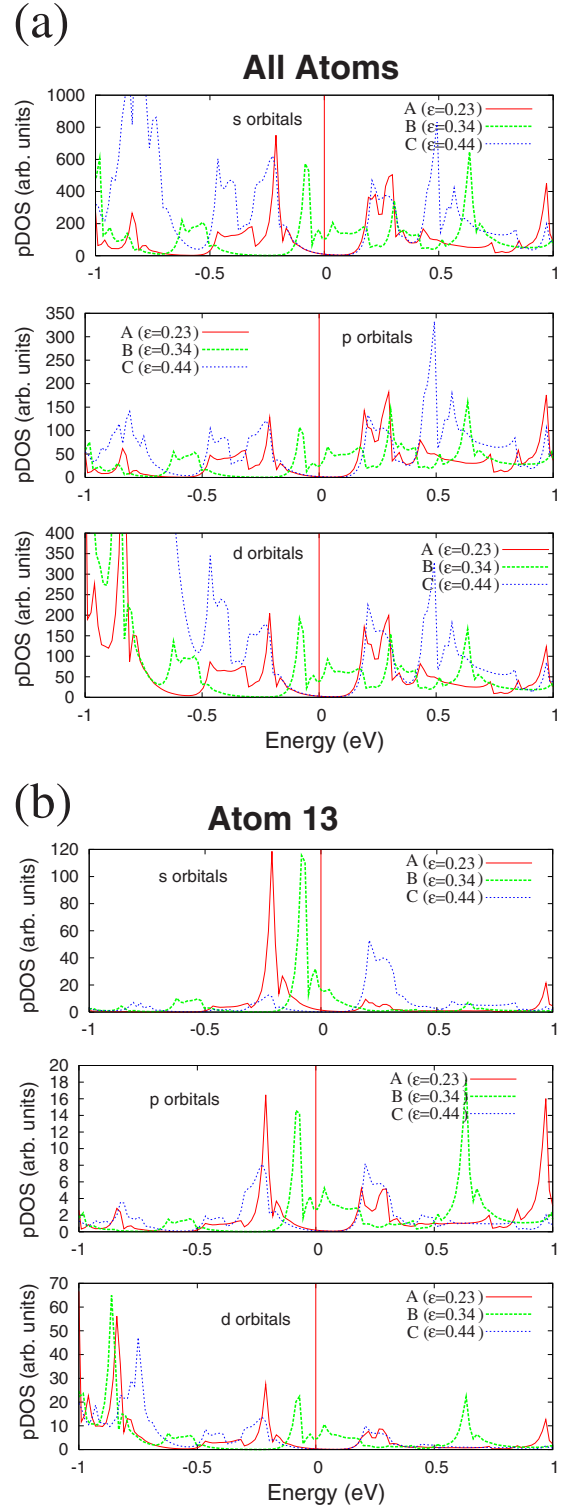


FIG. 13. (Color online) Projected density of states for the whole system (a), and for one of the atoms in the planar zigzag region (b) for structures A ($\epsilon=0.23$), B ($\epsilon=0.34$), and C ($\epsilon=0.44$) in Fig. 12. For each pDOS shown, the position of the Fermi energy is indicated by the vertical line.

states is raised well above the Fermi level, thus, reopening the band gap. This shifting of the energy level is consistent with the reduced delocalization of the electrons across the smaller number of atoms in the zigzag region.

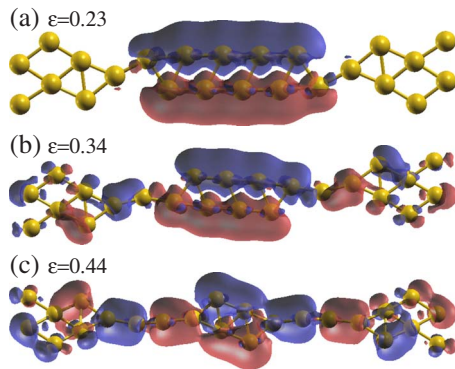


FIG. 14. (Color online) Atomic arrangements and HOMO (highest occupied molecular orbitals) isosurfaces for structures A ($\epsilon=0.23$), B ($\epsilon=0.34$), and C ($\epsilon=0.44$). Positive and negative lobes are colored blue and red, respectively, on line.

The binding between atoms in the central zigzag regions is very strong due to extensive orbital overlap in these planar substructures. It should be noted that there is significant p and d contribution to these bands, as well as the expected dominant s character. Due to the strong overlap between the atoms in the zigzag region, the resultant electronic states rise and fall together as a function of the length of the segment, thus strongly influencing conductivity along the nanowire.

IV. CONCLUSIONS

In this paper, we used semistatic DFT simulations to explore the structural and electronic behavior of Au NWs under

realistic conditions of imposed elastic and plastic strain. We find that the elastic and plastic strain are critical factors in evaluating the behavior of nanowires, both through determining the sequence of intermediate structures that evolve during deformation, and modifying the interactions of the electronic orbitals in wires that experience varying degrees of elastic strain. The sequence of structures that evolve during nanowire deformation depends upon three main factors: the presence of an energetically reasonable deformation path between consecutive structures (structural accessibility), stability under the imposed strain, and low energy under the constraint of fixed wire length and number of atoms.

These criteria were also examined for “reverse loading” conditions, where a NW is first deformed in tension and then deformed in compression. Here, although the sequence of encountered structures was only partially reversible, the same general rules applied. The electronic structure of the NWs was also found to be highly dependent upon the imposed strain, as typified by the previously reported semiconducting structure “ZZ3+5” for which the band gap varies dramatically with the imposed elastic strain. Most importantly, abrupt opening and closing of a band gap was observed during the plastic tensile deformation of several NWs, which may explain similar conductance oscillations observed experimentally. In one specific case that was examined in detail, the origin of this highly variable band gap was found to be caused by an increase in the energy of the occupied states (driven by reduced delocalization in a central region) through the Fermi level during deformation.

- ¹N. Agraït, J. G. Rodrigo, and S. Vieira, *Phys. Rev. B* **47**, 12345 (1993).
- ²G. Rubio, N. Agraït, and S. Vieira, *Phys. Rev. Lett.* **76**, 2302 (1996).
- ³C. Sirvent, J. G. Rodrigo, S. Vieira, L. Jurczyszyn, N. Mingo, and F. Flores, *Phys. Rev. B* **53**, 16086 (1996).
- ⁴H. van Houten and C. Beenakker, *Phys. Today* **49**(7), 22 (1996).
- ⁵J. L. Costa-Krämer, *Phys. Rev. B* **55**, R4875 (1997).
- ⁶H. Ohnishi, Y. Kondo, and K. Takayanagi, *Nature (London)* **395**, 780 (1998).
- ⁷V. Rodrigues and D. Ugarte, *Eur. Phys. J. D* **16**, 395 (2001).
- ⁸S. Tsukamoto, T. Ono, Y. Fujimoto, K. Inagaki, H. Goto, and K. Hirose, *Mater. Trans.* **42**, 2257 (2001).
- ⁹H. Mehrez, A. Wlasenko, B. Larade, J. Taylor, P. Grutter, and H. Guo, *Phys. Rev. B* **65**, 195419 (2002).
- ¹⁰M. Díaz, J. L. Costa-Krämer, E. Medina, A. Hasmy, and P. A. Serena, *Nanotechnology* **14**, 113 (2003).
- ¹¹L. G. C. Rego, A. R. Rocha, V. Rodrigues, and D. Ugarte, *Phys. Rev. B* **67**, 045412 (2003).
- ¹²I. K. Yanson, O. I. Shklyarevskii, S. Csonka, H. van Kempen, S. Speller, A. I. Yanson, and J. M. van Ruitenbeek, *Phys. Rev. Lett.* **95**, 256806 (2005).
- ¹³F. Tavazza, L. E. Levine, and A. M. Chaka, *J. Appl. Phys.* **106**, 043522 (2009).
- ¹⁴J. L. Costa-Krämer, N. García, P. García-Mochales, P. A. Serena, M. I. Marqués, and A. Correia, *Phys. Rev. B* **55**, 5416 (1997).
- ¹⁵G. Rubio-Bollinger, S. R. Bahn, N. Agraït, K. W. Jacobsen, and S. Vieira, *Phys. Rev. Lett.* **87**, 026101 (2001).
- ¹⁶C. Untiedt, A. I. Yanson, R. Grande, G. Rubio-Bollinger, N. Agraït, S. Vieira, and J. M. van Ruitenbeek, *Phys. Rev. B* **66**, 085418 (2002).
- ¹⁷V. Rodrigues and D. Ugarte, *Phys. Rev. B* **63**, 073405 (2001).
- ¹⁸Y. Takai, T. Kawasaki, Y. Kimura, T. Ikuta, and R. Shimizu, *Phys. Rev. Lett.* **87**, 106105 (2001).
- ¹⁹T. Kizuka, *Phys. Rev. B* **77**, 155401 (2008).
- ²⁰S. Tanimori, K. Ishida, O. Sueoka, and S. Shimamura, *J. Phys. Soc. Jpn.* **68**, 3556 (1999).
- ²¹S. P. Ju, J. S. Lin, and W. J. Lee, *Nanotechnology* **15**, 1221 (2004).
- ²²J. K. Diao, K. Gall, and M. L. Dunn, *J. Mech. Phys. Solids* **52**, 1935 (2004).
- ²³J. Diao, K. Gall, and M. L. Dunn, *Phys. Rev. B* **70**, 075413 (2004).
- ²⁴E. Z. da Silva, A. J. R. da Silva, and A. Fazzio, *Comput. Mater. Sci.* **30**, 73 (2004).
- ²⁵D. L. Chen and T. C. Chen, *Nanotechnology* **16**, 2972 (2005).
- ²⁶H. S. Park and J. A. Zimmerman, *Phys. Rev. B* **72**, 054106 (2005).
- ²⁷H. S. Park and J. A. Zimmerman, *Scr. Mater.* **54**, 1127 (2006).
- ²⁸J. K. Diao, K. Gall, M. L. Dunn, and J. A. Zimmerman, *Acta*

- Mater.* **54**, 643 (2006).
- ²⁹H. S. Park, K. Gall, and J. A. Zimmerman, *J. Mech. Phys. Solids* **54**, 1862 (2006).
- ³⁰S. J. A. Koh and H. P. Lee, *Nanotechnology* **17**, 3451 (2006).
- ³¹Q. Pu, Y. Leng, L. Tsetseris, H. S. Park, S. T. Pantelides, and P. T. Cummings, *J. Chem. Phys.* **126**, 144707 (2007).
- ³²F. Ma, S. L. Ma, K. W. Xu, and Paul K. Chu, *Nanotechnology* **18**, 455702 (2007).
- ³³D. Wang, J. Zhao, S. Hu, X. Yin, S. Liang, Y. Liu, and S. Deng, *Nano Lett.* **7**, 1208 (2007).
- ³⁴S. S. Liu, Y. H. Wen, and Z. Z. Zhu, *Chin. Phys. B* **17**, 2621 (2008).
- ³⁵K. Gall, J. K. Diao, M. L. Dunn, M. Haftel, N. Bernstein, and M. J. Mehl, *J. Eng. Mater. Technol.* **127**, 417 (2005).
- ³⁶F. Sato, A. S. Moreira, P. Z. Coura, S. O. Dantas, S. B. Legoas, D. Ugarte, and D. Galvão, *Appl. Phys. A: Mater. Sci. Process.* **81**, 1527 (2005).
- ³⁷R. Zoubkoff, L. de la Vega, A. Martin-Rodero, A. Levy Yeyati, and A. Saul, *Physica B* **398**, 309 (2007).
- ³⁸E. Z. da Silva, A. J. R. da Silva, and A. Fazzio, *Phys. Rev. Lett.* **87**, 256102 (2001).
- ³⁹E. Z. da Silva, F. D. Novaes, A. J. R. da Silva, and A. Fazzio, *Phys. Rev. B* **69**, 115411 (2004).
- ⁴⁰E. Z. da Silva, F. D. Novaes, A. J. R. da Silva, and A. Fazzio, *Nanoscale Res. Lett.* **1**, 91 (2006).
- ⁴¹D. Krüger, H. Fuchs, R. Rousseau, D. Marx, and M. Parrinello, *Phys. Rev. Lett.* **89**, 186402 (2002).
- ⁴²N. V. Skorodumova and S. I. Simak, *Phys. Rev. B* **67**, 121404(R) (2003).
- ⁴³N. V. Skorodumova, S. I. Simak, A. E. Kochetov, and B. Johansson, *Phys. Rev. B* **72**, 193413 (2005).
- ⁴⁴Abu Md. Asaduzzaman and M. Springborg, *Phys. Rev. B* **72**, 165422 (2005).
- ⁴⁵L. Ke, T. Kotani, M. van Schilfgaarde, and P. A. Bennett, *Nanotechnology* **18**, 424002 (2007).
- ⁴⁶F. Fioravante and R. W. Nunes, *Appl. Phys. Lett.* **91**, 223115 (2007).
- ⁴⁷N. V. Skorodumova, S. I. Simak, A. E. Kochetov, and B. Johansson, *Phys. Rev. B* **75**, 235440 (2007).
- ⁴⁸P. Seal and S. Chakrabarti, *Chem. Phys.* **335**, 201 (2007).
- ⁴⁹P. Vélez, S. A. Dassie, and E. P. M. Leiva, *Chem. Phys. Lett.* **460**, 261 (2008).
- ⁵⁰H. Ishida, *Phys. Rev. B* **77**, 155415 (2008).
- ⁵¹P. Jelínek, R. Pérez, J. Ortega, and F. Flores, *Phys. Rev. B* **77**, 115447 (2008).
- ⁵²W. Fa and J. Dong, *J. Chem. Phys.* **128**, 244703 (2008).
- ⁵³B. Wang, S. Yin, G. Wang, A. Buldum, and J. Zhao, *Phys. Rev. Lett.* **86**, 2046 (2001).
- ⁵⁴N. Agraït, A. L. Yeyati, and J. M. van Ruitenbeek, *Phys. Rep.* **377**, 81 (2003).
- ⁵⁵M. Springborg and Y. Dong, *Metallic Chains/Chains of Metals* (Elsevier, Amsterdam, 2007).
- ⁵⁶M. Dreher, F. Pauly, J. Heurich, J. C. Cuevas, E. Scheer, and P. Nielaba, *Phys. Rev. B* **72**, 075435 (2005).
- ⁵⁷M. Okamoto and K. Takayanagi, *Phys. Rev. B* **60**, 7808 (1999).
- ⁵⁸D. Sánchez-Portal, E. Artacho, J. Junquera, P. Ordejón, A. García, and J. M. Soler, *Phys. Rev. Lett.* **83**, 3884 (1999).
- ⁵⁹V. M. Garcia-Suarez, A. R. Rocha, S. W. Bailey, C. J. Lambert, S. Sanvito, and J. Ferrer, *Phys. Rev. Lett.* **95**, 256804 (2005).
- ⁶⁰F. J. Ribeiro and M. L. Cohen, *Phys. Rev. B* **68**, 035423 (2003).
- ⁶¹D. T. Smith, J. R. Pratt, F. Tavazza, L. E. Levine, and A. M. Chaka, *J. Appl. Phys.* **107**, 084307 (2010).
- ⁶²B. Delley, *J. Chem. Phys.* **92**, 508 (1990).
- ⁶³B. Delley, *J. Chem. Phys.* **113**, 7756 (2000).
- ⁶⁴M. N. Huda and A. K. Ray, *Eur. Phys. J. B* **43**, 131 (2005).
- ⁶⁵J. P. Perdew, K. Burke, and M. Ernzerhof, *Phys. Rev. Lett.* **77**, 3865 (1996).
- ⁶⁶B. Delley, *Phys. Rev. B* **66**, 155125 (2002).
- ⁶⁷P. Pulay and G. Fogarasi, *J. Chem. Phys.* **96**, 2856 (1992).
- ⁶⁸J. Baker, A. Kessi, and B. Delley, *J. Chem. Phys.* **105**, 192 (1996).
- ⁶⁹L. Fernández-Seivane, V. M. García-Suárez, and J. Ferrer, *Phys. Rev. B* **75**, 075415 (2007).
- ⁷⁰L. Xiao, B. Tollberg, X. Hu, and L. Wang, *J. Chem. Phys.* **124**, 114309 (2006).
- ⁷¹H. J. Monkhorst and J. D. Pack, *Phys. Rev. B* **13**, 5188 (1976).
- ⁷²P. Jelínek, R. Pérez, J. Ortega, and F. Flores, *Phys. Rev. Lett.* **96**, 046803 (2006); *Phys. Rev. B* **68**, 085403 (2003).
- ⁷³F. Picaud, A. Dal Corso, and E. Tosatti, *Surf. Sci.* **532-535**, 544 (2003).
- ⁷⁴N. W. Ashcroft and N. D. Mermin, *Solid State Physics* (Holt, Rinehart and Winston, New York, 1976).
- ⁷⁵S. M. Foiles, M. I. Baskes, and M. S. Daw, *Phys. Rev. B* **33**, 7983 (1986).
- ⁷⁶B. R. Sahu, G. Maofa, and L. Kleinman, *Phys. Rev. B* **67**, 115420 (2003).
- ⁷⁷*American Institute of Physics Handbook*, 3rd ed., edited by B. H. Billings and D. E. Gray (McGraw-Hill, New York, 1972).
- ⁷⁸J. Wang, G. Wang, and J. Zhao, *Phys. Rev. B* **66**, 035418 (2002).